Crystallization

Deutsche Ausgabe: DOI: 10.1002/ange.201507659
Internationale Ausgabe: DOI: 10.1002/anie.201507659

Precrystalline Aggregates Enable Control over Organic Crystallization in Solution

*Chen Shahar+, Sounak Dutta+, Haim Weissman, Linda J. W. Shimon, Holger Ott, and Boris Rybtchinski**

Abstract: *Understanding and controlling organic crystallization in solution is a long-standing challenge. Herein, we show that crystallization of an aromatic amphiphile based on perylene diimide in aqueous media involves initially formed amorphous spherical aggregates that evolve into the crystalline phase. The initial appearance of the crystalline order is always confined to the spherical aggregates that are precursors for crystalline evolution. The change in the solvation of the prenucleation phase drives the crystallization process towards crystals that exhibit very different structure and photofunction. The initial molecular structure and subsequent crystal evolution can be regulated by tuning the hydrophobicity at various stages of crystallization, affording dissimilar crystalline products or hindering crystallization. Thus, the key role of the precrystalline states in organic crystal evolution enables a new strategy to control crystallization by precrystalline state manipulation.*

Crystallization of organic molecules in solution is of primary importance in materials science, the pharmaceutical industry, and organic synthesis. However, controlling organic crystallization in solution has been a long-standing challenge,[1] and mechanistic insights into crystal evolution, especially into its early stages remains elusive.[2] There is emerging evidence that complex crystallization mechanisms, involving intermediate noncrystalline aggregates, often operate in inorganic, organic, and protein crystallization in solution.[3] Thus, a two-step nucleation mechanism[4] and the existence of prenucleation aggregates[5] (clusters) have been proposed to explain the discrepancies between classical nucleation theory and experiments. Direct imaging of prenucleation states is extremely challenging; it was achieved in inorganic crystallization[6] and in colloidal systems,[7] and, recently, in organic systems.[8] In general, the role of the initially formed amorphous phases in solution crystallization is not well understood, posing key questions of if and how the structures of these aggregates influence the crystallization process,[3a,5,9] and if they can be used to control crystallization. Herein, we show that the precrystalline phases play a key role in organic crystallization, and demonstrate that manipulating their structure and dynamics can regulate crystallization aptitudes, ultimately enabling control over organic crystallization.

Perylene diimides are widely utilized organic chromophores and semiconductors whose crystallization is of primary importance in device and pigment applications.[10] Compound **1** (Figure 1), a perylene diimide bearing an oxybenzoic acid substituent in the bay area, was chosen for our studies owing to its relatively slow crystallization in THF/aqueous solutions. We envisaged that such a slow rate may allow direct observation of precrystalline states, thus providing insights into their nature and evolution.

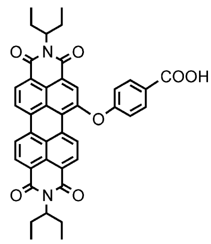

Figure 1. Structure of compound **1**.

The crystallization process of compound **1** was induced by the gradual addition of water to a concentrated solution of **1** in THF (2×10^{-3} M). Water was added dropwise (160 μL min^{-1}) at 23–25 °C by a syringe-pump under stirring to reach a 1×10^{-4} M concentration of compound **1** and 20% THF content by volume, resulting in a slightly turbid pink THF/water (1:4, v/v) solution (see the Supporting Information for details). The crystallization process was monitored using UV/Vis spectroscopy and electron microscopy. SEM, TEM, and cryo-TEM imaging revealed that immediately (1–2 min) after mixing THF and water, the solution contained spherical structures 200–600 nm in diameter (Figures 2a, S4a, S5a, S8). The spheres exhibited no apparent order and did not give rise to diffraction signals as observed by TEM and XRD (Figures 2a, S12). After approximately 15 min of aging, the smooth spherical boundaries become distorted, displaying edge-like features owing to the formation of thin sheet-like assemblies, which appeared within the sphere boundaries (Figures 2b, S4b,c, S5b, S6). The sheets exhibit crystalline order, as revealed by high magnification images (Figure 2b, inset). After approximately 30 min of aging, clusters of ruler-like crystals start to emerge from each sphere (Figures 2c, S5c, S8c,d). After 1 h of aging, the crystals are a few microns long, and begin to separate from one another (Figure S5d). The solution appears largely colorless after 24 h, and a red precipitate is observed, containing rectangular crystals 6–10 μm in length and 0.5–1 μm in width (Figures 2d,

[*] Dr. C. Shahar,[+] Dr. S. Dutta,[+] Dr. H. Weissman, Prof. B. Rybtchinski
Department of Organic Chemistry
Weizmann Institute of Science, Rehovot 76100 (Israel)
E-mail: boris.rybtchinski@weizmann.ac.il
Homepage: http://www.weizmann.ac.il/oc/boris/
Dr. L. J. W. Shimon
Department of Chemical Research Support
Weizmann Institute of Science (Israel)
Dr. H. Ott
Bruker AXS GmbH
Östliche Rheinbrückenstrasse 49, 76187 Karlsruhe (Germany)
[+] These authors contributed equally to this work.

Supporting information for this article is available on the WWW under http://dx.doi.org/10.1002/anie.201507659.

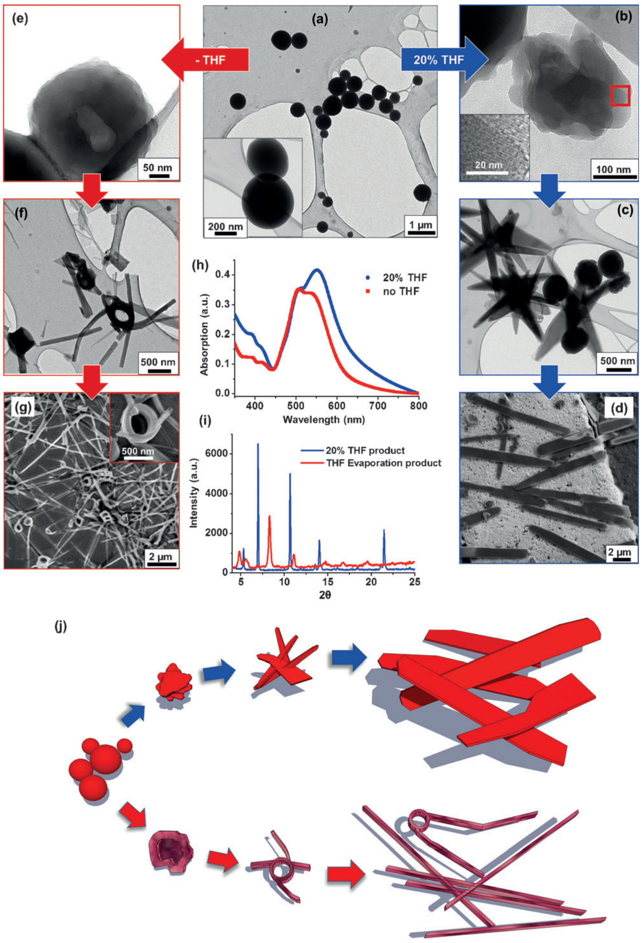

Figure 2. Crystal evolution in 20% THF solution (a–d) and in neat water after evaporating THF (a, e–g): a) TEM image of the initial amorphous aggregates; b) sheet-like crystalline structures, 15 min evolution (TEM); c) distorted spheres containing sheet-like crystals and crystalline clusters, 30 min evolution (TEM); d) final crystals, 24 h evolution (SEM); e) round structures following THF evaporation, 30 min evolution (TEM); f) intermediate stage: round barrel-like structures with crystals growing from them, 3 h evolution (TEM); g) final crystalline phase after 24 h (SEM); UV/Vis spectra (h) and XRD diffractograms (i) of the crystalline systems; j) illustration of the crystallization processes in 20% THF solution (blue arrows) and in neat water after evaporating THF (red arrows).

S5e, f), giving rise to sharp peaks in XRD diffractogram (Figures 2i, S12). Larger crystals, up to 100 µm in length and 10 µm in width, were also occasionally observed. The same crystalline evolution process was observed in multiple experiments. Importantly, the initial appearance of the crystalline order is always confined to the spherical aggregates, indicating that the latter are precursors for crystalline evolution.

UV/Vis spectra of **1** in THF/water (1:4, v/v) exhibited a red shift and broadening in comparison with the molecularly dissolved system (Figure 2h), and no significant spectral changes were observed throughout the crystal evolution process. Interestingly, 0-0/0-1 vibronic band inversion (indicative of face-to-face PDI stacking[10a]) did not occur, and no new red-shifted bands (characteristic of PDI slipped-stack formation in aqueous solutions[11]) were observed, suggesting that no significant interaction exists between PDI aromatic cores. Fluorescence emission spectra of the crystallization solution revealed an emission band peaking at 575 nm (Figure S2a). Notably, the fully assembled crystals are highly emissive (Figure S2c), having a quantum yield of ≈10%. To determine the crystal structure, we performed single-crystal X-ray diffraction studies. The molecules in the crystal (space group $P2_1/n$) are arranged in a herringbone motif where the phenyl substituent of the oxybenzoic acid group is involved in π-π interactions of 3.3 to 3.4 Å with the PDI cores of the neighboring molecules above and below it (Figure 3). The crystal structure is in agreement with the optical spectroscopy data, confirming no direct interaction between the PDI aromatic cores. Such a structure is not typical of PDI-based crystals, which usually feature interacting PDI cores.[10c]

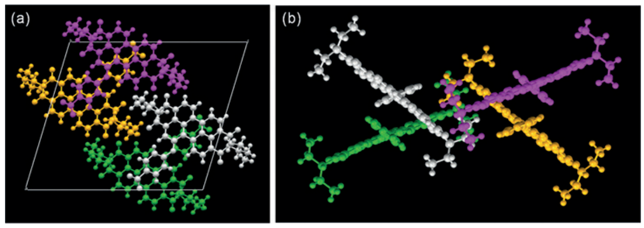

Figure 3. Single-crystal structure of **1** crystallized from a water/THF solution (4:1, v/v): a) top view of the unit cell containing 4 molecules; b) side view of the unit cell demonstrating π-stacking interactions between the phenyl substituent of one molecule and the perylene core of the adjacent molecule.

Our observations reveal that the formation of an amorphous phase precedes crystallization, and that crystallization is always initiated within this phase. This amorphous phase is relatively dense, as revealed from TEM images, yet it is dynamic and rearranges into a crystalline phase. In principle, the prenucleation phase, which lacks an inherent crystallization propensity, may be prone to changes regarding order evolution aptitudes. To address this notion, we evaporated THF at different stages of the crystallization process, occurring in a 1×10^{-4} M water/THF (4:1, v/v) solution of **1** (evaporation of THF under partial vacuum, followed by water addition to reach the original concentration conditions, see the Supporting Information). No significant change in the crystallization process was observed if THF was evaporated after the crystallization commenced (more than 30 min after the initial formation of spherical aggregates), yielding crystals with a structure and morphology identical to the 20% THF case, as evidenced by SEM and XRD (Figure S9). However, if THF is evaporated immediately after the formation of the aggregates, a strikingly different crystallization path occurs (Figure 2j). Here, the initially observed amorphous spheres become less dense at their center (Figure 2e), as indicated by TEM imaging. Crystalline order appears in the interior and at the exterior of these round structures after 3 h of aging (Figure 2f and Figure 4). The growth of short fiber-like crystals, originating at the circumference of the round-shaped structures (Figure 2f and Figure 4b) was also

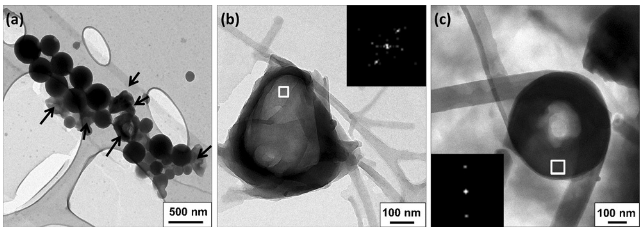

Figure 4. TEM images of the initial crystalline evolution, 15 min aging following THF evaporation (a,b): a) arrows point at distorted round structures that develop crystalline order; b) a magnified image of the intermediate crystallization stage. Inset = FFT of the marked area. c) A more developed round hollow structure with crystalline fibers growing from its circumference, 3 h after THF evaporation. Inset = FFT of the marked area.

observed. In the final crystalline phase the fiber-like crystals (several micrometers in length and 20–60 nm wide) precipitate after 24 h of aging (Figures 2g, S10, S11). Similar to the 20% THF system, the early formation of the crystalline phase is always localized within the boundaries of the initially formed amorphous aggregates, indicating their precursor role. Furthermore, the final crystalline phase is characterized by residual round-shaped spring-like and barrel-like crystalline structures (Figures 2g, 4c, S11a). These observations confirm that a direct structural connection exists between the aggregates and the crystals. The UV/Vis spectra of the crystalline phase exhibited substantial 0-0/0-1 vibronic band inversion (Figure 2h), typical of face-to-face PDI stacking.[10a] Consequently, the emission quantum yield of the crystals is significantly lower (≈1%) than the one observed for 20% THF crystals. XRD analysis of the crystalline product revealed a diffraction spectrum that was distinctly different from the 20% THF case (Figure 2i). Thus, the change in the solvation of the prenucleation phase drives the crystallization process towards producing crystals that exhibit very different short-range molecular interactions, packings, morphologies, and photofunctions. The observed change in the crystallization outcome is a result of stronger hydrophobic forces in neat water that drive the system to minimize the hydrophobic surface area (leading to PDI stacking) and, overall, resulting in a more compact structure.

We also observed that the molecular interactions in the precrystalline aggregates depend on the solvent mixing pathway, providing further insight into the connection between the initial amorphous phase and crystallization. The pathway described above, that is, the dropwise addition of water to the THF solution of **1**, leads to a UV/Vis spectrum without vibronic band inversion (Figure 5a, inset) and the initial formation of spherical aggregates (Figure 2a). Different mixing sequences, namely, the fast addition of either water to the THF solution of **1** or a THF solution of **1** to water (to reach 20% THF volume content; Figure S3c) results in the initial formation of amorphous structures, as revealed by TEM (Figure S16a), with the UV/Vis spectra displaying vibronic band inversion, indicative of PDI face-to-face stacking (Figure 5a). Apparently, these mixing pathways immediately impose a highly hydrophobic environment that induces a significant overlap of PDI aromatic cores, unlike in the case of dropwise water addition where hydrophobicity is increased gradually. Despite the different molecular interactions in the initial amorphous phase, we observed that the final crystalline products are almost identical in all pathways, differing slightly in morphology (Figures S13, S14). The crystallization process appeared to be faster in the dropwise addition path (1 day for the dropwise addition versus 5 days for the fast addition pathway). Evidently, kinetic barriers for crystal nucleation are higher in the fast addition pathways, owing to a significant molecular rearrangement that must occur: stacked PDI cores reorganize into a non-stacked crystal pattern. Thus, the structure of the precrystalline aggregates influences the crystallization rate; however, the systems are dynamic enough to evolve into identical crystals. To probe the effect of solvation on the fate of the initial phase obtained by different pathways, we evaporated THF (followed by re-addition of water to reach the original volume), immediately after the formation of precrystalline aggregates. As previously described, in neat water, the dropwise addition system develops into high aspect ratio crystals (Figure 2a, e–g). Remarkably, in the case of the fast addition pathways, crystallization was completely shut down by THF evaporation, and the initially formed spherical aggregates were stable for days (Figures 5b, S15a, b, S16b). Furthermore, seeding with preformed crystals did not influence the dynamics of the processes (no crystallization was observed), attesting to the stability of the aggregates. The difference in the behavior of the three precrystalline aggregate states in neat water can be explained by the difference in their molecular organization. Thus, only in the case of an aggregate where PDI aromatic surfaces do not interact (the dropwise addition path) did we observe crystallization, most probably owing to the highly energetically unfavorable structure in terms of hydrophobic hydration (Figure 5c). In two other cases, the aggregates featuring significant PDI stacking are more stable, since the kinetic barriers to their reorganization are higher because of strong hydrophobic interactions between the PDI cores.

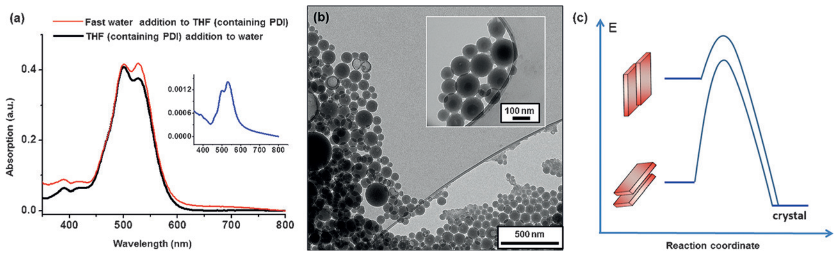

Figure 5. a) Normalized UV/Vis spectra of the assemblies formed in different mixing pathways. Red = fast water addition to THF; black = THF addition to water (inset = dropwise addition pathway). b) TEM image of the assembly formed by fast addition of THF to water, following THF evaporation and aging for 2 days. c) Schematic energy diagram depicting a high kinetic barrier for the crystallization of stacked PDI aggregates, and a lower kinetic barrier for non-stacked PDI structures.

Importantly, in neat water, unlike in the case of the THF/water mixture, the structure of the precrystallization aggregates defined the crystallization outcome. This is a consequence of the different dynamic ranges (reorganization propensities) of the system, which is influenced by solvation and is critical for controlling the initial molecular structure of the precrystalline phase and its subsequent evolution. The pathway-dependent formation of different precrystalline phases and their critical role in controlling crystallization are in agreement with the two-step crystallization mechanism.[3a,4b] Further insights into early stages of crystallization will be needed to elucidate how precrystalline states form, which may include a variety of precrystalline self-assembly and phase separation scenarios.[3a]

In summary, we observe that crystallization originates within the initially formed amorphous phase. We show that the propensity of this phase to crystallize critically depends on its structure and solvation, which can drive the crystallization process to different outcomes. Consequently, the initial molecular structure and subsequent crystal evolution can be regulated by hydrophobicity tuning at various stages of crystallization, affording dissimilar crystalline products, or even hindering crystallization. Manipulating the structure and dynamics of precrystalline phases represents a new strategy for understanding and controlling crystallization aptitudes, which may have broad implications for the area of organic crystalline materials.

CCDC 1416468 **1** contain the supplementary crystallographic data for this paper. These data can be obtained free of charge from The Cambridge Crystallographic Data Centre.

Acknowledgements

This work was supported by grants from the Israel Science Foundation, the Gerhardt M. J. Schmidt Minerva Center of Supramolecular Architecture, and the Helen and Martin Kimmel Center for Molecular Design. The EM studies were conducted at the Irving and Cherna Moskowitz Center for Nano and Bio-Nano Imaging (Weizmann Institute). S.D. acknowledges the PBC fellowship from the Council for Higher Education in Israel.

Keywords: crystallization · hydrophobic interactions · perylene diimide · polymorphism · prenucleation

How to cite: *Angew. Chem. Int. Ed.* **2016**, *55*, 179–182
Angew. Chem. **2016**, *128*, 187–190

[1] a) I. Weissbuch, M. Lahav, L. Leiserowitz, *Cryst. Growth Des.* **2003**, *3*, 125–150; b) J. D. Dunitz, J. Bernstein, *Acc. Chem. Res.* **1995**, *28*, 193–200; c) G. R. Desiraju, *J. Chem. Sci.* **2010**, *122*, 667–675; d) J. J. De Yoreo, P. G. Vekilov, *Biomineralization* **2003**, *54*, 57–93; e) A. G. Shtukenberg, S. S. Lee, B. Kahr, M. D. Ward, *Annu. Rev. Chem. Biomol. Eng.* **2014**, *5*, 77–96.

[2] P. G. Vekilov, *Nat. Mater.* **2012**, *11*, 838–840.

[3] a) J. J. De Yoreo, P. U. P. A. Gilbert, N. A. J. M. Sommerdijk, R. L. Penn, S. Whitelam, D. Joester, H. Zhang, J. D. Rimer, A. Navrotsky, J. F. Banfield, A. F. Wallace, F. M. Michel, F. C. Meldrum, H. Cölfen, P. M. Dove, *Science* **2015**, *349*, 498; b) R. P. Sear, *Int. Mater. Rev.* **2012**, *57*, 328–356; c) J. H. E. Cartwright, A. G. Checa, J. D. Gale, D. Gebauer, C. I. Sainz-Diaz, *Angew. Chem. Int. Ed.* **2012**, *51*, 11960–11970; *Angew. Chem.* **2012**, *124*, 12126–12137; d) S. Y. Chung, Y. M. Kim, J. G. Kim, Y. J. Kim, *Nat. Phys.* **2009**, *5*, 68–73.

[4] a) O. Galkin, P. G. Vekilov, *Proc. Natl. Acad. Sci. USA* **2000**, *97*, 6277–6281; b) P. G. Vekilov, *Nanoscale* **2010**, *2*, 2346–2357; c) P. R. tenWolde, D. Frenkel, *Science* **1997**, *277*, 1975–1978.

[5] D. Gebauer, M. Kellermeier, J. D. Gale, L. Bergstrom, H. Colfen, *Chem. Soc. Rev.* **2014**, *43*, 2348–2371.

[6] a) E. M. Pouget, P. H. H. Bomans, J. A. C. M. Goos, P. M. Frederik, G. de With, N. A. J. M. Sommerdijk, *Science* **2009**, *323*, 1455–1458; b) A. I. Lupulescu, J. D. Rimer, *Science* **2014**, *344*, 729–732; c) D. Gebauer, A. Volkel, H. Colfen, *Science* **2008**, *322*, 1819–1822.

[7] J. R. Savage, A. D. Dinsmore, *Phys. Rev. Lett.* **2009**, *102*, 198302.

[8] a) Y. Tidhar, H. Weissman, D. Tworowski, B. Rybtchinski, *Chem. Eur. J.* **2014**, *20*, 10332–10342; b) K. Harano, T. Homma, Y. Niimi, M. Koshino, K. Suenaga, L. Leibler, E. Nakamura, *Nat. Mater.* **2012**, *11*, 877–881.

[9] a) D. Erdemir, A. Y. Lee, A. S. Myerson, *Acc. Chem. Res.* **2009**, *42*, 621–629; b) R. J. Davey, S. L. M. Schroeder, J. H. ter Horst, *Angew. Chem. Int. Ed.* **2013**, *52*, 2166–2179; *Angew. Chem.* **2013**, *125*, 2220–2234.

[10] a) F. Würthner, *Chem. Commun.* **2004**, 1564–1579; b) F. Würthner, C. R. Saha-Möller, B. Fimmel, S. Ogi, P. Leowanawat, D. Schmidt, *Chem. Rev.* **2015**, DOI: 10.1021/acs.chemrev.1025b00188; c) X. W. Zhan, A. Facchetti, S. Barlow, T. J. Marks, M. A. Ratner, M. R. Wasielewski, S. R. Marder, *Adv. Mater.* **2011**, *23*, 268–284; d) E. Kozma, M. Catellani, *Dyes Pigm.* **2013**, *98*, 160–179; e) Y. Zhong, M. T. Trinh, R. S. Chen, W. Wang, P. P. Khlyabich, B. Kumar, Q. Z. Xu, C. Y. Nam, M. Y. Sfeir, C. Black, M. L. Steigerwald, Y. L. Loo, S. X. Xiao, F. Ng, X. Y. Zhu, C. Nuckolls, *J. Am. Chem. Soc.* **2014**, *136*, 15215–15221; f) B. A. Jones, M. J. Ahrens, M. H. Yoon, A. Facchetti, T. J. Marks, M. R. Wasielewski, *Angew. Chem. Int. Ed.* **2004**, *43*, 6363–6366; *Angew. Chem.* **2004**, *116*, 6523–6526; g) L. Schmidt-Mende, A. Fechtenkötter, K. Müllen, E. Moons, R. H. Friend, J. D. MacKenzie, *Science* **2001**, *293*, 1119–1122.

[11] J. Baram, H. Weissman, Y. Tidhar, I. Pinkas, B. Rybtchinski, *Angew. Chem. Int. Ed.* **2014**, *53*, 4123–4126; *Angew. Chem.* **2014**, *126*, 4207–4210.

Received: August 17, 2015
Revised: October 1, 2015
Published online: November 10, 2015

